Int J Thermophys (2010) 31:1234–1247
DOI 10.1007/s10765-010-0795-8

Characterization of Piezoelectric Ceramic Transducer for Accurate Speed-of-Sound Measurement

H. Lin · K. A. Gillis · J. T. Zhang

Received: 15 November 2009 / Accepted: 14 July 2010 / Published online: 30 July 2010

Abstract Piezoelectric ceramics mounted on the endplates of a cylindrical resonator were used as the source and detector for speed-of-sound measurements. The perturbations of the longitudinal gas modes of the cavity due to the compliance of the diaphragms (10 mm diameter, 0.3 mm thick) and the attached transducers were estimated from first-order perturbation theory. The fractional shift of the resonance frequencies in argon caused by the source and detector was 0.03×10^{-6} at 0.1 MPa and 273.16 K. The high signal-to-noise ratio (up to 1×10^4 with a 6 s integration time) that was obtained with these transducers makes them suitable for acoustic thermometry. The heat dissipation in the source transducer was measured to be only 0.7 μW at the working voltage (7 V) and frequency (1 kHz).

Keywords Acoustic thermometry · Cylindrical resonator · Piezoelectric ceramic transducer · Speed of sound

1 Introduction

Acoustic thermometry is one of the most accurate ways to determine the thermodynamic temperature and the Boltzmann constant. One measures the acoustic resonance frequencies of dilute, high purity argon, or helium in a gas-filled cavity [1–4].

H. Lin (✉) · J. T. Zhang
Division of Thermometry and Materials Evaluation, National Institute of Metrology (NIM), Beijing 100013, People's Republic of China
e-mail: linhong@nim.ac.cn

K. A. Gillis
Process Measurements Division, National Institute of Standards and Technology (NIST), Gaithersburg, MD 20899, USA
e-mail: keith.gillis@nist.gov

We plan to determine the universal gas constant R and the Boltzmann constant k_B with a relative uncertainty less than 1×10^{-6} in preparation for the new definition of the temperature unit—kelvin (K) [5]. In order to achieve this low uncertainty, the acoustic impedance of the transducer used to generate and detect the acoustic signal in the cavity needs to be determined over the whole working frequency range.

Quinn et al. [6,7] measured the Boltzmann constant using a variable-length cylinder resonator with a piezoelectric ceramic transducer as the detector. One obvious merit of their method was the high signal-to-noise ratio that compensated for the comparatively low-quality factor Q for the cylinder resonator. However, their method requires calculation of the perturbations to the acoustic and temperature fields for accurate determinations of the speed of sound and the Boltzmann constant.

In this article, lead zirconate titanate (PZT) piezoceramic transducers were attached to diaphragms on the endplates of a cylindrical cavity to generate and detect acoustic signals. We determined the acoustic impedance of the two transducers and the heat dissipation in the source transducer using experimental and theoretical techniques. We also calculated the perturbations of the resonance frequencies caused by the transducers and diaphragms. Because they dissipate very little heat and cause very small perturbations to the resonance frequencies, we conclude that piezoceramic transducers are suitable for use in acoustic thermometry.

2 Transducer Model

We constructed the piezoceramic-diaphragm system shown in Fig. 1 in the endplates of a cylindrical resonator. A thin diaphragm (0.3 mm thick), axially located, was machined into each endplate. A piezoelectric ceramic disk was bonded to the outer surface of each diaphragm with epoxy as shown in Fig. 1. One disk was used as an acoustic source and the other as a detector. The cylinder and endplates of the resonator were made from oxygen-free copper. The resonator had an inner radius of 40 mm, an inner length of 129.4 mm, and a wall thickness of 10 mm.

Gillis et al. [8] developed a model to estimate the source strength and detector sensitivity of piezoceramic-diaphragm transducers for acoustic measurements in xenon near its liquid-vapor critical point. The diaphragms used in [8] were 2.5 mm thick stainless steel to withstand the resonator's internal pressure of 6 MPa. Their analysis of their acoustic measurements showed that the displacement of the source diaphragm depended only on the applied voltage but not the drive frequency, characteristic of a high-impedance source. They found good agreement between the model and the experimental measurements of the source and detector responses. A slightly generalized version of the model[1] to include the impedance of the fluid is given in this section. A more rigorous model is given by Lihoreau et al. [9].

[1] K. A. Gillis, unpublished.

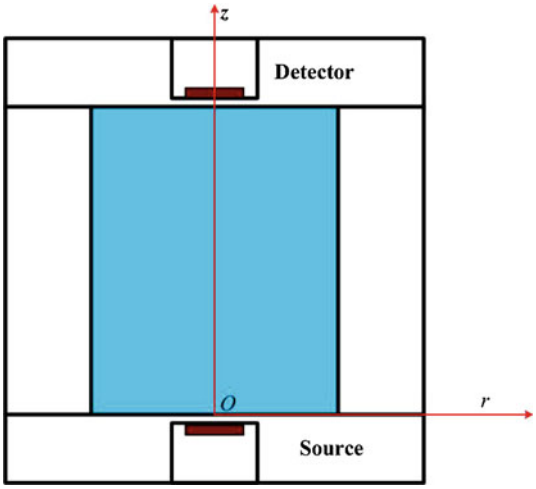

Fig. 1 Cylindrical resonator and transducer placement

2.1 Diaphragm Motion

We present a simple model for the low-frequency, long-wavelength response of a piezoceramic acoustic transducer when used as either a sound source or a detector. The transducer is composed of a piezoceramic bonded to a flexible diaphragm. The transducer behaves as a high-impedance sound source when a sinusoidal voltage is applied to the piezoceramic's electrodes. The deformation of the piezoceramic creates a stress on the diaphragm's surface that causes the diaphragm to deflect. When the diaphragm is driven by an acoustic pressure wave, a voltage is generated across the piezoceramic, and the transducer behaves as a sound detector. The frequency of the driven or detected sound is assumed to be much lower than the diaphragm's lowest resonance frequency, and the wavelength of sound in the gas is assumed to be much larger than the diaphragm's diameter.

Consider a circular diaphragm with strains in the diaphragm. A time-dependent force per unit area, $F_\omega e^{i\omega t}$, applied uniformly over the diaphragm will cause a displacement of the diaphragm in accordance with the force equation,

$$\sigma_d \ddot{\zeta} = -\frac{Y t_d^3}{12\left(1-\nu^2\right)} \nabla^4 \zeta + F_\omega e^{i\omega t} \tag{1}$$

where ζ is the instantaneous deflection of the plate in the z-direction as a function of the distance r from the axis, σ_d is the areal mass density, Y is Young's modulus, ν is Poisson's ratio, and the over-dot signifies time differentiation. A "clamped" boundary condition is appropriate here. When the frequency $f = \omega/2\pi$ is much lower than the diaphragm's resonance frequency, the diaphragm's inertia is negligible, and the amplitude of the displacement is approximately [10]

$$\zeta(r) \approx \frac{3\left(1-\nu^2\right) F_\omega a^4}{16 Y t_d^3} \left[1 - \left(\frac{r}{a}\right)^2\right]^2 + \cdots \tag{2}$$

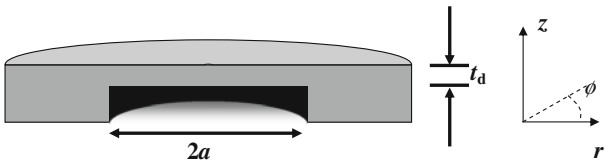

Fig. 2 Pressure applied on a diaphragm

We consider two contributions to F_ω: stress from the piezoceramic F_{PZT} due to an applied voltage and the acoustic pressure $\tilde{p}$ generated in front of the diaphragm. These contributions oppose each other, so the total force per unit area is $F_\omega = F_{\mathrm{PZT}} - \tilde{p}$. Note that a positive acoustic pressure $\tilde{p}$ above the diaphragm in Fig. 2 causes a negative deflection.

Since, we are interested only in the low-frequency, long-wavelength limit, we need only consider the average deflection over the area of the plate

$$\langle \zeta \rangle = \frac{1}{\pi a^2} \int_0^a \zeta(r) 2\pi r \mathrm{d}r \approx \frac{\left(1 - v^2\right) F_\omega a^4}{16 Y t_\mathrm{d}^3}. \tag{3}$$

The compliance per unit area of the diaphragm $\chi_\mathrm{F} = \langle \zeta \rangle / F_\omega$ is a measure of the diaphragm displacement resulting from an applied force. The compliance in this limit is approximately

$$\chi_\mathrm{F} \approx \frac{(1 - v^2) a^4}{16 Y t_\mathrm{d}^3}. \tag{4}$$

The compliance is an important parameter that is used to estimate the perturbation on the gas modes in a resonant cavity. A complete dynamical treatment shows that the compliance is frequency-dependent and becomes very large when the frequency is near one of the diaphragm's resonance frequencies. A large compliance may result in an unacceptably large perturbation of the gas modes of an acoustic resonator, especially if the diaphragm and gas mode frequencies are close together. Our model is valid for operating frequencies much lower than the lowest diaphragm resonance frequency.

In response to a sinusoidal driving voltage applied to the piezoceramic, the deflection of the diaphragm displaces a volume of gas at an average rate given by

$$U_\mathrm{src} = \mathrm{i}\omega\pi a^2 \langle \zeta \rangle . \tag{5}$$

An important property of an acoustic source is the mechanical impedance per unit area $Z_\mathrm{m} = F_\omega / U_\mathrm{src}$. The mechanical impedance of a good volume-velocity source is large when compared to the acoustic impedance of the medium in which the acoustic wave is generated. The acoustic pressure $\tilde{p}$ generated at the endplate by this volume velocity source in a cavity is proportional to the acoustic impedance of the gas in the cavity Z_cav, i.e.,

$$\tilde{p} = U_{\mathrm{src}} Z_{\mathrm{cav}} = \mathrm{i}\omega\pi a^2 \chi_{\mathrm{F}} Z_{\mathrm{cav}} \left(F_{\mathrm{PZT}} - \tilde{p}\right). \tag{6}$$

Therefore, the acoustic pressure generated in the cavity acts to oppose the stress in the diaphragm that drives the diaphragm's motion. The resultant acoustic pressure is, therefore,

$$\tilde{p} = \frac{\mathrm{i}\omega\pi a^2 \chi_{\mathrm{F}} Z_{\mathrm{cav}} F_{\mathrm{PZT}}}{1 + \mathrm{i}\omega\pi a^2 \chi_{\mathrm{F}} Z_{\mathrm{cav}}} = \frac{Z_{\mathrm{cav}}}{Z_{\mathrm{m}} + Z_{\mathrm{cav}}} F_{\mathrm{PZT}}. \tag{7}$$

The frequency-dependent impedance Z_{cav} is the response of the gas in the cavity and includes the line shapes of the resonances. The magnitude of Z_{cav} has peaks at the resonance frequencies. At the resonance frequency $f_l = \omega_l/2\pi$ of a longitudinal mode in a cylindrical cavity, the cavity impedance is

$$Z_{\mathrm{cav}}(\omega_l) = \frac{2\rho c^2}{V} \frac{Q_l}{\omega_l}, \tag{8}$$

where ρ is the gas density, c is the speed of sound in the gas, V is the cavity volume, and Q_l is the quality factor of the resonance. Equation 8 follows from the resonator response calculated from the Green's function as discussed in Sect. 3 below. If the ratio $Z_{\mathrm{cav}}/Z_{\mathrm{m}}$ is small in the vicinity of the resonance, then the measured response will closely approximate the resonance's true line shape. For the resonators and transducers studied here, we estimate that Z_{m} is at least 100 times larger than Z_{cav} for frequencies up to 16 kHz.

2.2 Electromechanical Model

In order to relate the motion of the diaphragm to the voltages that are either applied to or generated at the pioezoceramic electrodes, we must estimate the stresses in the diaphragm and in the piezoceramic. The stresses in the diaphragm as a function of distance from the center due to an applied force per unit area F_ω are approximately [10]

$$\sigma_r = \frac{3}{8}\left(\frac{a}{t_{\mathrm{d}}}\right)^2 \left[(1+v) - (3+v)\left(\frac{r}{a}\right)^2\right] F_\omega \tag{9}$$

$$\sigma_\theta = \frac{3}{8}\left(\frac{a}{t_{\mathrm{d}}}\right)^2 \left[(1+v) - (1+3v)\left(\frac{r}{a}\right)^2\right] F_\omega \tag{10}$$

where σ_r and σ_θ are the radial and the azimuthal stresses, respectively. The radial and azimuthal strains in the diaphragm are, respectively,

$$\varepsilon_r = \frac{1}{Y}\left(\sigma_r - v\sigma_\theta\right) \tag{11}$$

and

$$\varepsilon_\theta = \frac{1}{Y}\left(\sigma_\theta - \upsilon\sigma_r\right). \tag{12}$$

Similar relationships hold for the strains in the piezoceramic in terms of the PZT's Young's modulus Y_{PZT} and Poisson's ratio υ_{PZT}. We equate the radial strains and the azimuthal strains in the diaphragm and the ceramic, $\varepsilon_r = (\varepsilon_r)_{\mathrm{PZT}}$ and $\varepsilon_\theta = (\varepsilon_\theta)_{\mathrm{PZT}}$, since the two materials are bonded together. These relationships can be inverted to give relationships between the stresses in the ceramic and in the diaphragm,

$$(\sigma_r)_{\mathrm{PZT}} = \frac{Y_{\mathrm{PZT}}}{\left(1-\upsilon_{\mathrm{PZT}}^2\right)}\left[(\varepsilon_r)_{\mathrm{PZT}} + \upsilon_{\mathrm{PZT}}(\varepsilon_\theta)_{\mathrm{PZT}}\right] = \frac{Y_{\mathrm{PZT}}}{Y}\sigma_r \tag{13}$$

$$(\sigma_\theta)_{\mathrm{PZT}} = \frac{Y_{\mathrm{PZT}}}{\left(1-\upsilon_{\mathrm{PZT}}^2\right)}\left[(\varepsilon_\theta)_{\mathrm{PZT}} + \upsilon_{\mathrm{PZT}}(\varepsilon_r)_{\mathrm{PZT}}\right] = \frac{Y_{\mathrm{PZT}}}{Y}\sigma_\theta. \tag{14}$$

For a circular piezoelectric ceramic disk that has been poled along the z-axis (perpendicular to the flat faces), the relevant piezoelectric coefficients that relate the stresses and strains to the electric fields are

$$\frac{\Delta a_{\mathrm{PZT}}}{a_{\mathrm{PZT}}} = 2d_{31}E_z \quad E_z = g_{31}\left[(\sigma_r)_{\mathrm{PZT}}\right]_{r=a_{\mathrm{PZT}}} \tag{15}$$

where $\left[(\sigma_r)_{\mathrm{PZT}}\right]_{r=a_{\mathrm{PZT}}}$ is the radial stress at $r = a_{\mathrm{PZT}}$, E_z is the electrical field in the z direction, and the coupling matrices d_{ij} and g_{ij} contain the piezoelectric properties of the piezoceramic. Equation 15 are obtained from the constitutive equations [11].

From Eq. 15, the radial strain in the diaphragm at $r = a_{\mathrm{PZT}}$ is given by

$$\left[(\varepsilon_r)_{\mathrm{PZT}}\right]_{r=a_{\mathrm{PZT}}} = \frac{\Delta a_{\mathrm{PZT}}}{a_{\mathrm{PZT}}} = (\varepsilon_r)_{r=a_{\mathrm{PZT}}} \tag{16}$$

where a_{PZT} is the radius of the piezoelectric ceramic. The strain in the piezoceramic due to the applied voltage produces in the diaphragm a similar strain that results in the diaphragm deflection. From Eqs. 9 and 10, we obtain a relationship between the strain generated in the diaphragm and the force per unit area $F_\omega = F_{\mathrm{PZT}}$ generated by the piezoceramic,

$$(\varepsilon_r)_{r=a_{\mathrm{PZT}}} = \frac{1}{Y}\frac{3}{8}\left(\frac{a}{t_{\mathrm{d}}}\right)^2\left(1-\upsilon^2\right)\left[1-3\left(\frac{a_{\mathrm{PZT}}}{a}\right)^2\right]F_{\mathrm{PZT}}. \tag{17}$$

Combining Eqs. 15–17, and the relationship between the electric field and the applied voltage $E_z = V_{\mathrm{s}}/t_{\mathrm{PZT}}$, we find

$$F_{\mathrm{PZT}} = \frac{16}{3}\frac{d_{31}V_{\mathrm{s}}}{t_{\mathrm{PZT}}}\left(\frac{t_{\mathrm{d}}}{a}\right)^2 Y\frac{1}{\left(1-\upsilon^2\right)\left[1-3\left(a_{\mathrm{PZT}}/a\right)^2\right]}. \tag{18}$$

Substituting Eqs. 4, 8, and 18 into Eq. 7 in the limit that $Z_m \gg Z_{cav}$, we obtain

$$\tilde{p}_l = \frac{2iQ_l\rho c^2}{3R^2L}\frac{a^4}{t_{PZT}t_d}\frac{d_{31}V_s}{\left[1-3\left(a_{PZT}/a\right)^2\right]} \tag{19}$$

for the acoustic pressure amplitude at the endplate of a cylindrical resonator as a function of the voltage amplitude applied to the source transducer at the frequency f_l of the lth longitudinal mode. R and L are the radius and length of the cylindrical cavity, respectively.

Next, we estimate the sensitivity of the detector to an incident acoustic pressure $\tilde{p}$. From Eqs. 9 and 13 with $F_\omega = -\tilde{p}$, the radial stress in the PZT detector as a function of r is

$$(\sigma_r)_{PZT} = \frac{Y_{PZT}}{Y}\sigma_r = \frac{Y_{PZT}}{Y}\frac{3}{8}\left(\frac{a}{t_d}\right)^2\left[(3+v)\left(\frac{r}{a}\right)^2-(1+v)\right]\tilde{p}. \tag{20}$$

The voltage from the detector V_d is

$$\begin{aligned} V_d &= \langle E\rangle_{PZT}\, t_{PZT} = t_{PZT}\frac{1}{\pi a_{PZT}^2}\int_0^{a_{PZT}} g_{31}\,(\sigma_r)_{PZT}2\pi r\,dr \\ &= t_{PZT}g_{31}\frac{Y_{PZT}}{Y}\frac{3}{16}\left(\frac{a}{t_d}\right)^2\left[(3+v)\left(\frac{a_{PZT}}{a}\right)^2-2(1+v)\right]\tilde{p} \end{aligned} \tag{21}$$

where $\tilde{p}$ is the RMS acoustic pressure. We combine Eqs. 19 and 21 to obtain an estimate of the detector signal V_d at a longitudinal resonance in the cylindrical cavity as a function of the RMS source voltage V_s

$$\begin{aligned} V_d = {} & ig_{31}d_{31}V_sQ_l\rho c^2\frac{Y_{PZT}a^6}{8Yt_d^3R^2L} \\ & \times\left[(3+v)\left(\frac{a_{PZT}}{a}\right)^2-2(1+v)\right]\left[1-3\left(\frac{a_{PZT}}{a}\right)^2\right]^{-1}. \end{aligned} \tag{22}$$

For the resonator and transducers used in this study, Eq. 22 predicts the RMS detector signal to be about 50 μV for 1 V (RMS) applied to the source when the resonator is filled with argon at 0.1 MPa.

3 Piezoceramic Transducers in a Cylindrical Resonator

In this section, we investigate some practical aspects of the piezocermaic transducers for use in a cylindrical resonator to measure the Boltzmann constant: (1) optimal transducer placement, (2) perturbations of the resonance frequencies, (3) dissipation in the source transducer, and (4) the signal-to-noise ratio. The piezoelectric ceramics

Table 1 Properties of PKI-402 PZT

Name	Unit	Values
Radius	m	0.0032
Thickness	m	0.0004
Transverse charge coefficient d_{31}[a]	$\mathrm{m \cdot V^{-1}}$	-120×10^{-12}
Transverse voltage coefficient g_{31}[a]	$\mathrm{m \cdot V \cdot N^{-1}}$	-10.8×10^{-3}
Young's modulus[a]	GPa	76
Poisson ratio[a]		0.31

[a] Data supplied by the manufacturer

used in this article were made of lead zirconate titanate (Navy Type I, PKI-402) from Piezo Kinetics Inc.[2] The properties of PKI-402 PZT ceramic are shown in Table 1.

3.1 Location of the Source and Detector

Consider the motion of a gas in a closed cylindrical cavity with radius R and length L. We use $\mathbf{r}$ to specify points within the cavity and $\mathbf{r_w}$ to specify points on the boundary. The source and detector are embedded in the endplate as described in the previous section. The source is approximated as a piston centered at $\mathbf{r} = \mathbf{r_0}$ with area πa^2 and velocity $\mathbf{u_{src}} = -\hat{\mathbf{n}} U_{\mathrm{src}}/\pi a^2$, where $\hat{\mathbf{n}}$ is the outward-pointing normal to the wall and U_{src} is the volume velocity defined in the previous section. The effects of heat transport and viscosity near the wall are included in the boundary condition as a nonuniform specific acoustic admittance $y_w(\omega, \mathbf{r_w})$. The steady-state acoustic pressure $\tilde{p}_\omega$ in the cavity, when the source is driven at frequency ω, is the solution to the Helmholtz equation [12,13];

$$\nabla^2 \tilde{p}_\omega(\mathbf{r}) + (\omega/c)^2 \tilde{p}_\omega(\mathbf{r}) = 0, \tag{23}$$

with the condition at $\mathbf{r} = \mathbf{r_w}$ that $\hat{\mathbf{n}} \cdot \nabla \tilde{p}_\omega = -i(\omega/c)\ y_w\ \tilde{p}_\omega - i\omega\rho u_{\mathrm{src}}$ for $\mathbf{r_w}$ within the source area and $\hat{\mathbf{n}} \cdot \nabla \tilde{p}_\omega = -i(\omega/c)\ y_w\ \tilde{p}_\omega$ for $\mathbf{r_w}$ outside the source area. The acoustic pressure at the location of the detector $\mathbf{r_d}$ is given by the formal solution,

$$\tilde{p}_\omega(\mathbf{r_d}) = -\mathrm{i}\omega\rho \sum_N \frac{\Psi_N(\mathbf{r_d}) \int_S \Psi_N(\mathbf{r}')\, \hat{\mathbf{n}} \cdot \tilde{\mathbf{u}}_{\mathrm{src}}(\omega, \mathbf{r}')\ \mathrm{d}S'}{\Lambda_N V \left[(2\pi F_N/c)^2 - (\omega/c)^2\right]}, \tag{24}$$

where the normal mode Ψ_N is an eigenfunction of $\nabla^2 \Psi_N + (2\pi F_N/c)^2 \Psi_N = 0$ with $\hat{\mathbf{n}} \cdot \nabla \Psi_N = -\mathrm{i}(\omega/c)\ y_w\ \Psi_N$ everywhere on the boundary [12,13]. The wavefunction Ψ_N and the complex-valued normal-mode frequency $F_N = f_N + i g_N$ formally

[2] In order to describe materials and experimental procedures adequately, it is occasionally necessary to identify commercial products by the manufacturer's name or label. In no instance does such identification imply endorsement by the National Institute of Metrology or the National Institute of Standards and Technology; nor does it imply that the particular product or equipment is necessarily the best available for the purpose.

include the effects of the thermoacoustic boundary layer. f_N and g_N are the observed resonance frequency and half-width, respectively, of the Nth normal mode of the gas-filled cavity. The parameter $\Lambda_N = (1/V)\int_V \Psi_N^2 \mathrm{d}V$ is a normalization constant.

The source and detector transducers are not point objects, but they are small when compared to the wavelength of sound. Since we assume a piston-like source (u_{src} is constant over the source's area and zero elsewhere), the integration over $\Psi_N(\mathbf{r}')\hat{\mathbf{n}} \cdot \mathbf{u_{src}}(\mathbf{r}')$ in Eq. 24 becomes $\pi a^2 \hat{\mathbf{n}} \cdot \mathbf{u_{src}} \langle \Psi_N(\mathbf{r_0}) \rangle_{\mathrm{src}}$, where $\langle \Psi_N(\mathbf{r_0}) \rangle_{\mathrm{src}}$ is the average of the wave function over the area of the source at $\mathbf{r_0}$. The signal from the detector transducer at $\mathbf{r_d}$ is proportional to $\langle \tilde{p}_\omega(\mathbf{r_d}) \rangle_{\mathrm{d}}$, the average of the acoustic pressure over the area of the detector. We average both sides of Eq. 24 and replace $\Psi_N(\mathbf{r_d})$ with its average $\langle \Psi_N(\mathbf{r_d}) \rangle_{\mathrm{d}}$. In terms of these average quantities, the detector signal is proportional to

$$\langle \tilde{p}_\omega(\mathbf{r_d}) \rangle_{\mathrm{d}} = \frac{\rho c^2 U_{\mathrm{src}}}{2\pi V} \sum_N \frac{\text{if } \langle \Psi_N(\mathbf{r_d}) \rangle_{\mathrm{d}} \langle \Psi_N(\mathbf{r_0}) \rangle_{\mathrm{src}}}{\Lambda_N \left(F_N^2 - f^2\right)}. \tag{25}$$

Equation 25 contains a sum over the lineshapes of all the modes of the cavity. In the vicinity of a resonance that is well separated from other modes, the sum can be approximated by a single resonance term plus a sloping background. For such high-Q modes, the dominant frequency dependence comes from the resonance denominator, and the effect of the boundary admittance y_w on Ψ_N can be neglected for the purpose of studying transducer placement.

The eigenfunctions for the rigid-walled ($y_w = 0$) resonator are [12,13]

$$\Psi_{lmn}(\mathbf{r}) = J_m(\chi_{mn} r/R)\,[\cos(m\phi) + \sin(m\phi)]\cos(l\pi z/L), \tag{26}$$

where J_m is the mth-order cylindrical Bessel function, and χ_{mn} is a solution of $J'_m(\chi_{mn}) = 0$. We specify the normal modes of the gas by the triplet of integers $(l|m|n)$, where $l = 0, 1, 2, \ldots$ is the longitudinal quantum number, $m = 0, \pm 1, \pm 2, \ldots$ is the azimuthal quantum number, and $n = 0, 1, 2, \ldots$ is the radial quantum number.[3] With this convention, $(l00)$ denotes the modes with z-dependence only (longitudinal modes), $(0|m|0)$ denotes the modes with ϕ-dependence only (azimuthal modes), and $(00n)$ denote the modes with r-dependence only (radial modes). All other modes are called mixed modes. When $|m| > 0$, the eigenfunctions with azimuthal quantum numbers $\pm|m|$ are doubly degenerate.

If the thermal and viscous boundary layer corrections are assumed to be the only perturbations, the real and imaginary parts of the acoustic pressure are obtained from first-order perturbation theory [12,13]:

[3] The notation we use was adopted from [13], Sect. 9.2, which describes the modes of circular ducts. The mode designated $(l|m|n)$ has l nodal planes perpendicular to the cylindrical axis, $|m|$ nodal planes extending radially from the axis, and n cylindrical nodal surfaces concentric with the axis. Our notation differs from that of [12] for which the third number in the triplet $n' = n + 1$.

$$\mathrm{Re}\,\langle p_\omega(\mathbf{r}_\mathrm{d})\rangle_\mathrm{d} = \frac{\rho c^2 U_\mathrm{src}}{2\pi V}\frac{\delta_\mathrm{T}}{R}\sum_{lmn}\frac{A_{lmn} f^3 \Omega_{lmn}}{\left[f_{0,lmn}^2 - f^2\left(1+\frac{\delta_\mathrm{T}}{R}\Omega_{lmn}\right)\right]^2 + \left(f^2\frac{\delta_\mathrm{T}}{R}\Omega_{lmn}\right)^2} \tag{27}$$

$$\mathrm{Im}\,\langle p_\omega(\mathbf{r}_\mathrm{d})\rangle_\mathrm{d} = \frac{\rho c^2 U_\mathrm{src}}{2\pi V}\sum_{lmn}\frac{A_{lmn} f\left[f_{0,lmn}^2 - f^2\left(1+\frac{\delta_\mathrm{T}}{R}\Omega_{lmn}\right)\right]}{\left[f_{0,lmn}^2 - f^2\left(1+\frac{\delta_\mathrm{T}}{R}\Omega_{lmn}\right)\right]^2 + \left(f^2\frac{\delta_\mathrm{T}}{R}\Omega_{lmn}\right)^2}, \tag{28}$$

where

$$A_{lmn} = (-1)^l \varepsilon_l \frac{J_m(\chi_{mn}a/R)\, J_m(\chi_{mn}b/R)\,[\cos(m\phi_\mathrm{d}) + \sin(m\phi_\mathrm{d})]}{\left[1-(m/\chi_{mn})^2\right] J_m^2(\chi_{mn})} \tag{29}$$

and

$$\Omega_{lmn} = \frac{\gamma-1}{1-(m/\chi_{mn})^2}\left[1+\frac{\varepsilon_l R}{L}\left(1-\frac{m^2}{\chi_{mn}^2}\right)\right] + \frac{\sqrt{\mathrm{Pr}}}{1-(m/\chi_{mn})^2}\left[1-\frac{\chi_{mn}^2-m^2}{(l\pi R/L)^2+\chi_{mn}^2}\left(1-\frac{\varepsilon_l R}{L}\right)\right] \tag{30}$$

Here, $f_{0,lmn}$ is the unperturbed resonance frequency, δ_T is the thickness of the thermal boundary layer, γ is the heat capacity ratio, and Pr is the Prandtl number. ε_l is defined to be 1 for $l = 0$ and 2 for $l > 0$.

The theoretical response from Eqs. 27–30 predicts that the coupling between the transducers and a particular mode (and therefore the observed response) will be minimum (maximum) when the transducers are placed at a pressure node (antinode) for that mode. To test this prediction, we measured the acoustic spectrum of the cylindrical resonator (Fig. 1), filled with argon at 0.1 MPa and 293.16 K, with the source transducer placed at two different locations: (1) the center of the endplate, $(r, \phi, z) = (0, 0, 0)$, to maximize the coupling to the longitudinal and radial modes while minimizing the coupling to the azimuthal modes, and (2) off center at $(r, \phi, z) = (0.628R, 0, 0)$, which is at a radial node for the modes $(l01)$ for $l = 0, 1, 2, \ldots$ In both the cases, the detector was located on the axis at the opposite end of the resonator, i.e., $(r, \phi, z) = (0, 0, L)$. The top of Fig. 3 shows the measured frequency response between 1 kHz and 6.5 kHz for case (1) with both transducers located on the axis. The longitudinal modes $(l00)$, the radial mode (001), and the mixed modes $(l01)$ are clearly visible. The azimuthal modes near 2334 Hz, 3872 Hz, and 5326 Hz do not appear, since the coupling of these modes to both transducers is weak. The bottom of Fig. 3 shows the response for case (2) over the same frequency range as the top one in Fig. 3. The radial and mixed mode amplitudes have been reduced by a factor of 200 due to the reduced coupling. The azimuthal modes again do not appear since the coupling to the detector is weak.

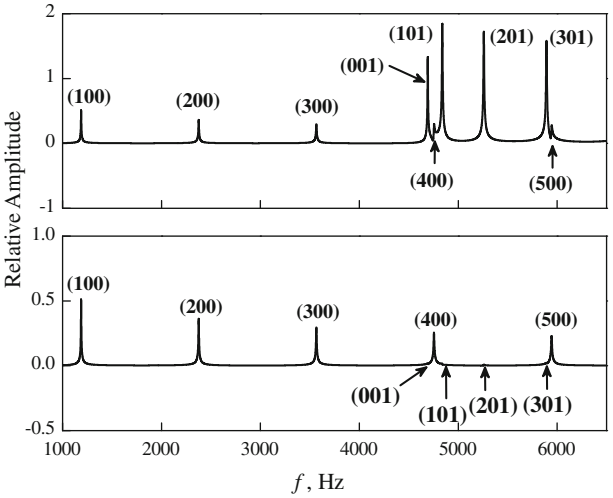

Fig. 3 Spectrum of modes between 1 kHz and 6.5 kHz of a cylindrical cavity (80 mm in diameter and 129.4 mm long) filled with argon at 293.16 K and 0.1 MPa. *Top* source and detector transducers are centered on opposite endplates; *bottom* source transducer is located at a pressure node for the first radial mode $(r, \phi, z) = (0.628R, 0, 0)$ of the endplate. Radial mode (001) and mixed modes (101), (201), and (301) are not present due to inefficient coupling to the sound source. Note the different vertical scale from the top figure.

3.2 Compliance and Perturbation of the Transducer

The diaphragm's compliance χ_F in the low-frequency limit is given in Eq. 4. The acoustic admittance of the diaphragm as seen by a wave in the resonator is [1]

$$y_{tr} = i\omega\rho c\chi_F. \tag{31}$$

We use first-order perturbation theory to estimate the frequency shift for the ideal longitudinal modes [14];

$$\frac{\Delta f_{tr}}{f_0} = \frac{i y_{tr} A_{tr}}{l\pi^2 R^2} = -\frac{\rho c^2 \chi A_{tr}}{\pi R^2 L} \tag{32}$$

where f_0 is the the ideal resonance frequency in the cavity. Table 2 shows the estimated perturbations for a 0.64 cm (1/4 inch) microphone and the PKI-402 PZT transducer at 273.16 K and different pressures. The perturbations for the microphone are calculated using data from Ref. [1] for a spherical cavity resonator with an inner radius of 9 cm.

3.3 Heat Generated by the PZT

We measured the dissipation in one of the PZT transducers while it was attached to the diaphragm in the endplate as indicated in Fig. 1. Figure 4 shows the circuit we

Table 2 Perturbations for the PZT transducer and condenser microphone

	$\frac{\Delta f_{\rm tr}}{f_0}/10^{-6}$	
	0.1 MPa	1 MPa
0.64 cm (1/4 inch) Microphone	−0.16	−1.60
PKI-402 PZT	−0.03	−0.27

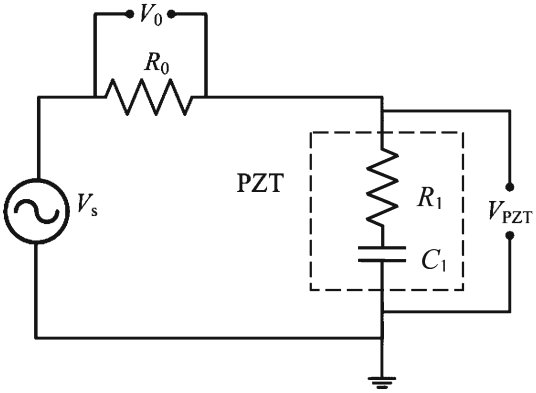

Fig. 4 Circuit used to measure the dissipation factor

used to measure the dissipation factor tan δ as a function of voltage and frequency. The equivalent circuit for the PZT element is assumed to be a series combination of resistance R_1 and capacitance C_1, which is shown inside the dash frame in Fig. 4. The PZT's capacitance was 600 pF. The standard resistor $R_0 = 200.110\ \Omega$, which was used to measure the current in the circuit, had negligible capacitance and inductance. The voltages across the standard resistor and across the PZT element were measured with a dual-phase lock-in. We determined the power dissipation from the expression,

$$P_{\rm diss} = \frac{V_0}{R_0} V_{\rm PZT} \cos\theta, \tag{33}$$

where $\theta = \pi/2 - \delta$ is the phase angle between the current and $V_{\rm PZT}$. Figure 5 shows the dissipation as a function of the square of source voltage V_s^2 at different frequencies. When the PZT is operated at 7 V (RMS), the dissipation in the transducer varies from 0.75 μW to 35 μW when the frequency varies from 1 kHz to 15 kHz based on extrapolation of the values shown in Fig. 5. The empirical function,

$$\frac{P_{\rm diss}}{\mu\rm W} = 5.14 \times 10^{-3} \left(\frac{f}{\rm kHz}\right)^{1.83} \left(\frac{V_{\rm PZT}}{V}\right)^2 \tag{34}$$

correlates the frequency, voltage, and dissipation data with an uncertainty of 6 nW.

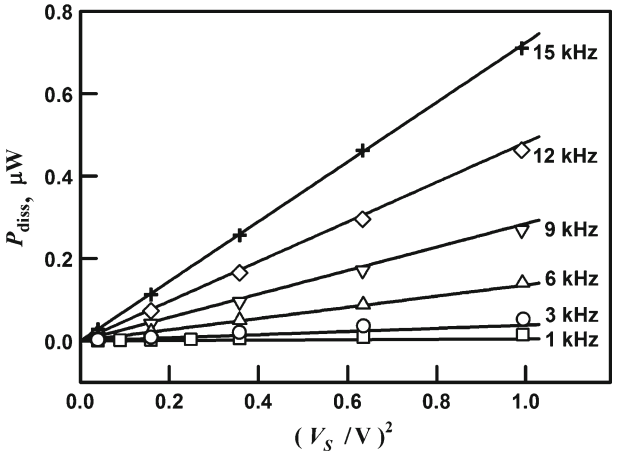

Fig. 5 Power dissipation of the PKI-402 PZT as a function of the square of the source voltage between 1 kHz and 15 kHz. *Solid lines* are fits given by Eq. 34.

3.4 Signal-to-Noise Ratio

Piezoelectric ceramic transducers can improve the signal-to-noise ratio for measurements in the cylinder resonator. The top of Fig. 6 shows a typical acoustic resonance for which the resonance frequency and half-width were $F_N = f_N + \mathrm{i}g_N = 1976.4072 + \mathrm{i}1.7668$ Hz. These data were acquired with an integration time of 6 s at each frequency. We measured the frequencies and half-widths of the longitudinal resonances in argon at 0.1 MPa and also used the fitting method described by Moldover

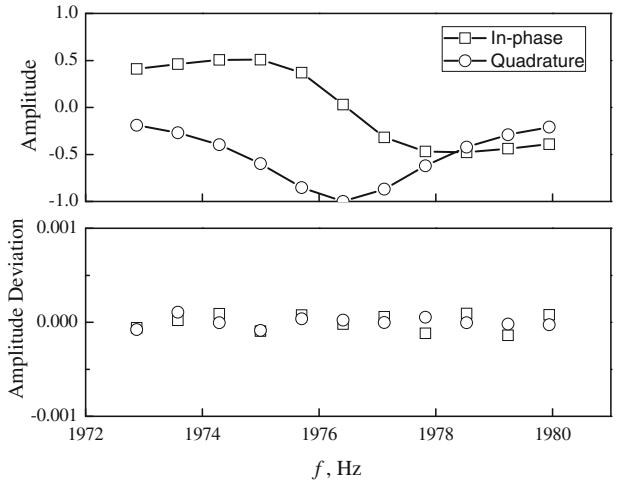

Fig. 6 *Top* in-phase and quadrature voltages from the PZT detector as a function of frequency near the (100) longitude mode of our cylinder resonator ($2R = 80$ mm, $L = 80$ mm) in argon at 0.1 MPa and 293.15 K; *bottom* measured voltages minus calculated voltages [15].

et al. [15]. The bottom of Fig. 6 shows the amplitude deviation for the in-phase and quadrature components. The signal-to-noise ratio is more than 1×10^4.

4 Conclusions

Piezoceramic transducers made from PKI-402 PZT are suitable to generate and detect sound for acoustic thermometry. The piezoelectric ceramic transducers were set on the middle of each endplate to minimize the coupling to the azimuthal modes. We observed a signal-to-noise ratio up to 1×10^4 for our cylinder resonator which is high enough to fit the complex resonance frequency with a precision of 10^{-7} of f_N. With an RMS drive voltage of 7 V, dissipation in the piezoceramic transducer varied from 0.75 μW to 35 μW when the frequency varied from 1 kHz to 15 kHz. The fractional frequency perturbations to the longitudinal modes were estimated to be only -0.03×10^{-6} and -0.27×10^{-6} for pressures of 0.1 MPa and 1 MPa, respectively, at 273.16 K in argon.

Acknowledgments The authors are grateful to M. R. Moldover for his technical comments, suggestions, and continuing assistance in this project. This study was supported by the National Natural Science Foundation of China (No. 50906076) and the National Science & Technology Pillar Program (2006BAF06B00) in China.

References

1. M.R. Moldover, J.P.M. Trusler, T.J. Edwards, J.B. Mehl, R.S. Davis, J. Res. Natl. Bur. Stand. **93**, 85 (1988)
2. M.R. Moldover, S.J. Boyes, C.W. Meyer, A.R.H. Goodwin, J. Res. Natl. Inst. Stand. Technol. **104**, 11 (1999)
3. G. Benedetto, R.M. Gavioso, R. Spagnolo, P. Marcarino, A. Merlone, Metrologia **41**, 74 (2004)
4. L. Pitre, M.R. Moldover, W.L. Tew, Metrologia **43**, 142 (2006)
5. B. Fellmuth, C. Gaiser, J. Fischer, Meas. Sci. Technol. **17**, R145 (2006)
6. T.J. Quinn, A.R. Colclough, T.R.D. Chandler, Philos. Trans. R. Soc. Lond. A **283**, 367 (1976)
7. A.R. Colclough, T.J. Quinn, T.R.D. Chandler, Proc. R. Soc. Lond. A **368**, 125 (1979)
8. K.A. Gillis, I.I. Shinder, M.R. Moldover, Phys. Rev. E **70**, 021201 (2004)
9. B. Lihoreau, P. Lotton, M. Bruneau, V. Gusev, Acta Acust. United Acust. **88**, 986 (2002)
10. R.J. Roark, *Formulas for Stress and Strain* (McGraw-Hill, New York, 1965)
11. J.M. Herbert, *Ferroelectric Transducers and Sensors* (Gordon and Breach, New York, 1982)
12. J.P.M. Trusler, *Physical Acoustics and Metrology of Fluids* (Hardcover, Bristol, 1991)
13. P.M. Morse, K.U. Ingard, *Theoretical Acoustics* (McGraw-Hill, New York, 1968)
14. K.A. Gillis, H. Lin, M.R. Moldover, J. Res. Natl. Inst. Stand. Technol. **114**, 263 (2009)
15. M.R. Moldover, J.B. Mehl, M. Greenspan, J. Acoust. Soc. Am. **79**, 253 (1986)